Generation of additive colors with near unity amplitude using a multilayer tandem Fabry–Perot cavity

Ali Cahit Kosger[1,2*], Amir Ghobadi[1,3], Alireza Rahimi Rashed[4], Humeyra Caglayan[4], Ekmel Ozbay[1,2,3*]

[1]*NANOTAM-Nanotechnology Research Center, Bilkent University, 06800 Ankara, Turkey*
[2]*UNAM - National Nanotechnology Research Center, Institute of Materials Science and Nanotechnology, Bilkent University, 06800 Ankara, Turkey*
[3]*Department of Electrical and Electronics Engineering, Bilkent University, 06800 Ankara, Turkey*
[4]*Faculty of Engineering and Natural Sciences, Photonics, Tampere University, 33720 Tampere, Finland*
**Corresponding authors: kosger@bilkent.edu.tr, Ozbay@bilkent.edu.tr*
Received XX Month XXXX; revised XX Month, XXXX; accepted XX Month XXXX; posted XX Month XXXX (Doc. ID XXXXX); published XX Month XXXX

In this paper, the generation of additive red-green-blue (RGB) colors in reflectance mode with near unity amplitude is demonstrated. For this purpose, a multilayer structure, made of metal-insulator-metal-semiconductor-insulator (MIMSI) stacks, is designed to achieve >0.9 reflection peaks with full-width-at-half-maximum (FWHM) values <0.3λ_{peak}. The proposed design also shows near zero reflection in off-resonance spectral ranges which, in turn, leads to high color purity. The optimized designs have been fabricated and the simulation and theoretical results have been verified with characterization findings. This work demonstrates the potential of multilayer tandem cavity designs in the realization of lithography-free large scale compatible functional optical coatings.

http://dx.doi.org/10.1364/OL.99.099999

Inspired by natural photonic designs such as Morpho butterfly, structural coloring based on nanophotonics and nanoplasmonics designs has been the subject of many studies in recent years [1]. In an ideal scheme, a color filter selectively transmits/reflects/absorbs a narrow wavelength range while it has weak light-matter interaction in non-resonant regions. Up to now, various design architectures have been utilized to fabricate color filters in reflection and transmission modes. Designs operating based on surface plasmon resonance [2–6], guided-mode resonance [7–11], and photonic crystals [12,13], and other innovative ideas [14,15] are some of these approaches. However, in all of these designs, the color generation is accomplished via spectrally selective light-matter interaction in sub-wavelength metal/dielectric nanounits. The realization of these nanounits, however, requires complex fabrication routes, such as electron-beam lithography (EBL), and nano-imprint lithography (NIL) which are large-scale incompatible approaches. Thus, lithography-free design structures have attracted much attention in recent years [16].

Among all, metal-insulator (MI) pair based Fabry-Perot (FP) resonators are the most commonly employed designs for a large-scale color generation [17–26]. These multilayer designs provide strong interference in spectrally selective regions. Generally, these planar designs produce additive red-green-blue (RGB) colors in transmission mode and subtractive cyan-magenta-yellow (CMY) colors in reflection mode. Unlike reflection mode designs that can reach near unity amplitude, transmissive RGB colors have efficiencies lower than ~0.7, due to the existence of multiple lossy layers in their propagation path. To tackle this deficiency, proposing a planar lithography-free architecture to generate RGB colors in the reflection mode is a possible solution. The use of lossy metals such as bismuth [27] , and nickel [28] as the top layer in a metal-insulator-metal (MIM) design has been proposed to achieve this goal. However, the wide full-width-at-half-maximum (FWHM) of these designs reduces the color purity. Other innovative architectures have been also explored to generate RGB colors in reflection mode but their efficiency were also much below unity [29].

In this letter, the generation of RGB colors is numerically and experimentally demonstrated using a designed metal-dielectric medium. For this purpose, first, a modeling approach based on transfer matrix method (TMM) is developed to compare the performance of common MIM cavities with those of metal-insulator-metal-insulator (MIMI) ones. Later, using numerical simulations, the optimal geometries are extracted. Gaining knowledge from these results, a hybrid structure made of metal-insulator-metal-semiconductor-insulator (MIMSI) stacks, is optimized to create RGB colors with high purity and near unity amplitude. Finally, the optimal geometries are utilized to fabricate RGB color filters with >0.9 reflection peak and FWHM <0.3λ_{peak}. The findings of this study shows that a proper connection of cavities in a tandem scheme can offer diverse functionalities that cannot be realized with conventional FP resonators.

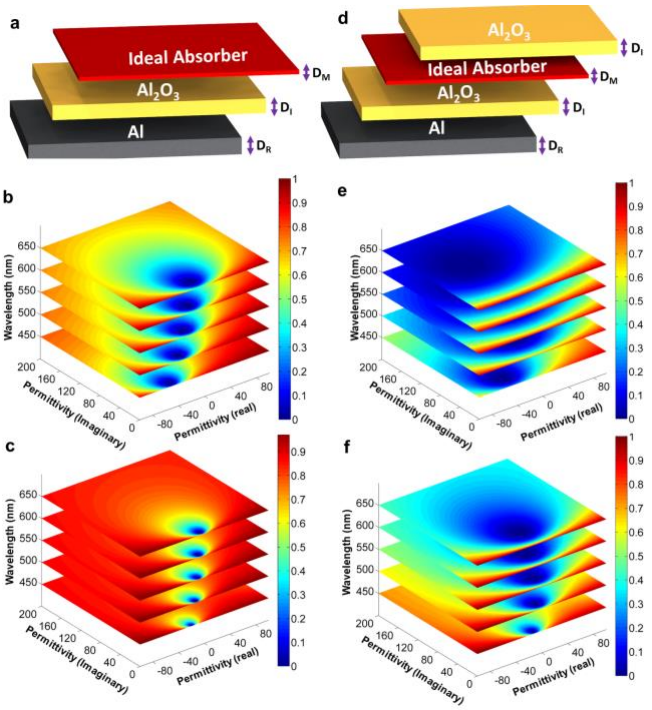

Fig. 1. Schematic representation of **(a)** MIM cavity design. The reflection contour plots of a MIM cavity at different real and imaginary permittivity values for D_M of **(b)** 5 nm, and **(c)** 15 nm. Schematic representation of **(d)** MIMI cavity design. The reflection contour plots of a MIM cavity at different real and imaginary permittivity values for D_M of **(e)** 5 nm, and **(f)** 15 nm. In all modelling results, the (D_I) is set as 60 nm Al_2O_3 layer and bottom layer is an optically thick Al layer. The color bar shows the reflection value of the cavity.

To begin with, the reflection characteristics of two common FP resonators of MIM and MIMI are scrutinized using a modelling approach based on TMM, see Figs. 1(a)-1(f). The details of this modelling have been explained in our previous studies [33]. In this modelling the bottom layer is fixed as an optically thick aluminum mirror, the spacer thickness (D_I) is set as 60 nm Al_2O_3 layer, and the reflection contour plots for different top metal thicknesses (D_M) of 5 nm and 15 nm are extracted. These contour plots have been obtained for five different wavelength values of 450 nm, 500 nm, 550 nm, 600 nm, and 650 nm. In these 2D plots, the centric blue semi-circles shows the real and imaginary permittivity values, required to have <0.1 reflection (absorption >0.9). Comparing these two designs, it can be understood that the tolerable region for light perfect absorption is wider for the MIMI design (compared to that of MIM). Moreover, thicker D_M values lead to wider perfect absorption circles. Also, these circles are placed at vicinity of center and a lossy metal with real and imaginary parts close to zero will provide better performance. Thus, from these modelling findings, in a MIMI absorber made of a lossy metal, constructive interference at a specific wavelength will lead to near unity reflection, while the other parts of the spectrum will be perfectly absorbed. By this way, an RGB color filter, in the reflective mode, with high efficiency and color purity is generated.

To verify these modelling outputs and to find the optimal geometries of the RGB color filter, the numerical simulations, using Lumerical finite-difference-time-domain (FDTD) software package, are performed [30]. In the FDTD simulations, we illuminated the unit cell with a broadband plane wave at normal incidence. In the simulations, the bottom layer is chosen as 150 nm thick Al layer. The insulator layers are set as Al_2O_3 with identical thicknesses of D_I. Finally, the top metal layer is Ni with thickness of D_M. All the permittivity data are extracted from Palik model [31]. In this design, two main geometries of D_I and D_M are

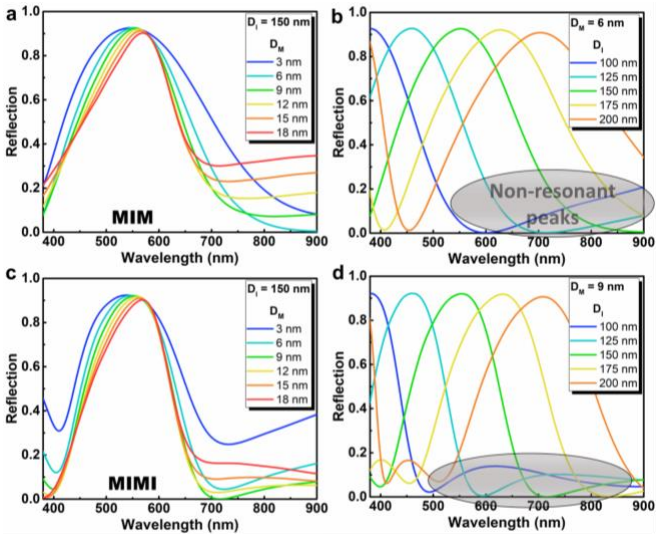

Fig. 2. The reflection spectra of MIM cavity design for different **(a)** D_I and **(b)** $D_M$values. The reflection spectra of MIMI design for different **(c)** D_I and **(d)** D_M values. The highlighted regions show the non-resonant ripples.

responsible for the optical behavior of the cavities. Thus, the impact of these two factors are separately studied for both MIM and MIMI cavities. First, the insulator layer thickness is fixed and metal layer is swept to find the optimal value for light perfect absorption. Later, the metal layer thickness is fixed at the optimum value, and the spectral shift of this resonance peak in different insulator layer thicknesses is studied. As shown in Fig. 2(a), for MIM design, D_I is fixed at 150 nm and D_M is swept from 3 nm to 18 nm, with a step of 5 nm. As this panel implies, the reflection peak amplitude is almost constant for all metal thicknesses. But, as we go toward thicker layers, the FWHM gets narrower. However, at the expense of this narrowing, the non-resonant response (reflection ripples in the non-resonant spectral range) becomes larger and this, in turn, reduces the color purity of the filter. Thus, in an appropriate metal thickness layer, we can provide a right trade-off between these two factors. This trade-off is satisfied in $D_M = 6$nm for the MIM cavity absorber. Setting this as the top layer, next, D_I is swept from 100 nm to 200 nm (with 25 nm step). From Fig. 2(b), the reflection peak is monolithically shifted from blue to red wavelengths, without any loss in its amplitude. However, blue filters (lower wavelength ranges) suffer from non-resonant absorptions (in longer visible range) and this will lead to poorer color pureness. A similar analysis is performed on MIMI cavity absorber, as shown in Figs. 2(c)-2(d). For MIMI color filters, the optimal D_M is 9 nm. Comparing with MIM cases, MIMI designs have smaller FWHM but similar to them they also have non-resonant absorption ripples and therefore, they have low color vividness.

Considering all the above findings, the MIMI configuration based color filters have better performance in RGB color generation, compared to that of MIM ones. However, both designs have poor color purity and using a conventional single cavity FP resonator, this property cannot be achieved. Thus, simultaneous realization of color purity and efficiency needs a tandem scheme FP design. Back to modelling data proposed in Fig 1(f), to have near zero reflection in all wavelength values, we need to approach the effective permittivity of metal layer to the zero center. In other words, instead of a single metal, we can use an effective metal-dielectric double layer to reduce the effective permittivity values toward lower ones. For this purpose, a multilayer design based on metal-insulator-metal-semiconductor-insulator (MIMSI) stacks is developed, as seen in Fig. 3(a). The semiconductor layer is Ge with a thickness of 3 nm. All other geometries are set at the optimal values of MIMI structure. The reflection spectra of MIMI and MIMSI designs are compared in Fig. 3(b). As this figure depicts, the

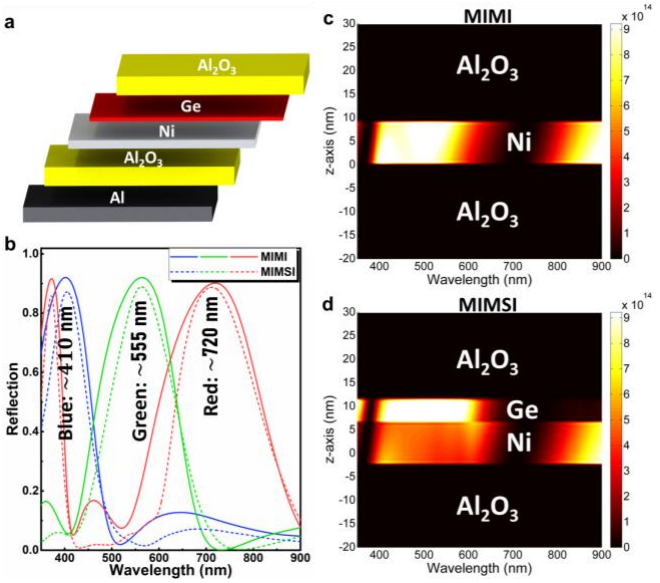

Fig. 3. (a) The schematic representation of MIMSI cavity design, **(b)** the reflection spectra of RGB color filters for MIMI and MIMSI structures, the absorption profile across the cavity structure for **(c)** MIMI and **(d)** MIMSI color filters. The color bar shows the absorbed power value.

addition of an ultrathin Ge layer not only lowered the FWHM of the reflection peak but also effectively mitigated the non-resonant absorption ripples. To understand the function of this Ge layer on the overall optical performance of MIMSI FP cavity, the absorbed power across the MIMI and MIMSI cavities has been plotted in Figs. 3(c)-3(d). It should be mentioned that in these contour plots the profile is zoomed on the active middle layer and this data belongs to the case of red filter. From these panels, the Ge layer harnessed most of the incoming power in the shorter λ values and Ni is the active material in the longer ranges, while both of these layers are transparent in the peak resonance position. This can be seen from the linear plots as well (Fig. 3(b)), where the sub-peaks (non-resonant modes) in reflection of MIMI is suppressed by MIMSI design. Thus, using this designed FP resonator, it is possible to achieve large scale compatible, and high efficiency RGB vivid colors in the reflection mode color filters.

Gaining insight into the design operation of the proposed MIMSI FP cavity and optimizing its performance using numerical simulations, in the next step, these simulation data has to be verified by experimental data. For this aim, a set of MIMSI samples with optimized D_M values of 9 nm and different D_I thicknesses (from 110 nm to 200 nm by a step of 15 nm) are fabricated using cleanroom facilities. To have a better qualitative comparison with a common FP color filter, a similar set is also fabricated for MIM architecture. For the fabrication, Si wafer is diced into 1cm× 1cm pieces and standard cleaning process is applied on them. The metallic (both Al and Ni) and Ge layers are coated at the desired thicknesses, using the thermal evaporation technique. The deposition rate was set at around 1.5-2 A°/s for all layers and the chamber pressure was kept below 5e-6 Torr throughout the deposition process. For Al_2O_3 coating, atomic layer deposition (Cambridge Nanotech Savannah S100) is used at 250 ^{0}C using $Al(CH_3)_3$ and water precursors as aluminum and oxygen sources. The pulse and purge times are chosen to be 0.015 s and10 s. The optical image of fabricated MIM and MIMSI samples is present in Fig. 4(a). From their visual appearance, it can be deduced that MIMSI cavities have better color vividness, compared to MIM ones. To verify the formation of different layers, scanning electron microscopy (SEM) imaging is utilized. Cross sectional SEM images of the MIM and MIMSI samples, shown in Figs. 4(b)-4(c), confirms successful growth of all layers. After initial structural analysis, optical characterizations are utilized to probe the reflection response of each sample. To measure the

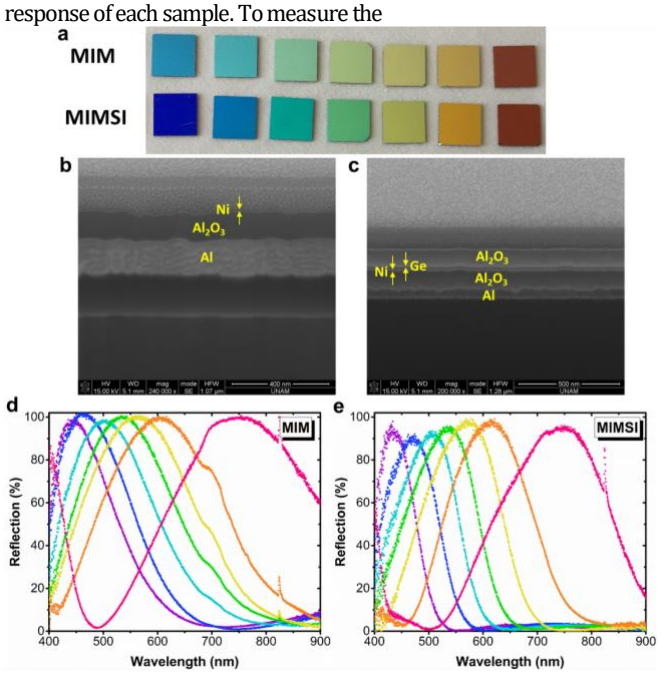

Fig. 4. (a) The optical image of MIM and MIMSI samples with different spacer thicknesses to generate RGB colors. The cross sectional SEM image of the **(b)** MIM, and **(c)** MIMSI cavity designs. The measured reflection spectra of different **(d)** MIM, and **(e)** MIMSI samples.

normal incidence reflection, in the wavelength range of 0.4–0.9 μm, we used an in-house setup comprising a halogen lamp as the incident light source, where this source was integrated into a microscope to collect the reflected light from the surface. As it can be seen from Fig. 4(d), the MIM color filter have reflection peaks above 0.95. This peak value is gradually reduced but it still stays above 0.9 for MIMSI cavity designs, see Fig. 4(e). However, in a one-by-one comparison, it can be found that MIMSI designs have considerably lower FWHMs and quite small non-resonance reflection colors. For instance, in the case of the blue color filter (for D_I =110 nm), the FWHM for MIM and MIMSI samples are 131 nm (0.3λ_{peak}) and 77 nm (0.17λ_{peak}), respectively. These values for green color (D_I =155 nm) are found to be 231 nm (0.43λ_{peak}) and 141 nm (0.43λ_{peak}) and red color (D_I =200 nm) are 323 nm (0.43λ_{peak}), and 228 nm (0.3λ_{peak}), for MIM and MIMSI samples, respectively.

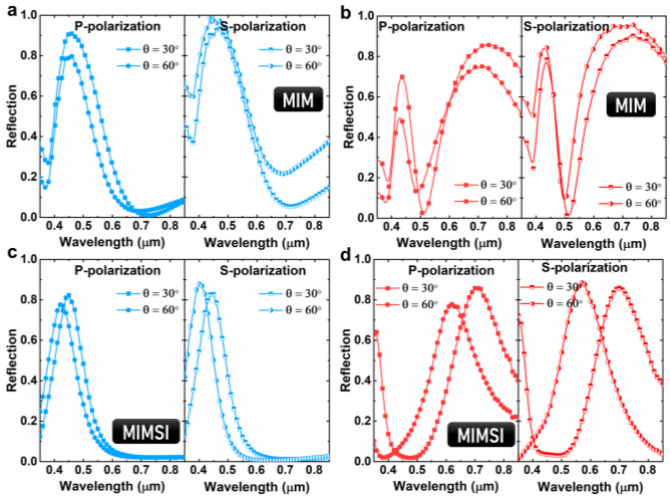

Fig. 5. The angular response of the MIM filter for two different colors of **(a)** blue, and **(b)** red. The angular response of the MIMSI structure for two different colors

of **(c)** blue, and **(d)** red. The measurements are carried out at both p and s polarizations and two different incident angles of 30^0, and 60^0.

Another factor that should be considered in the performance analysis of these FP filters is their angular response. For this aim, ellipsometry measurements are carried out in two incidence angles of 30^0 and 60^0 at S and P polarizations for both MIM and MIMSI designs with blue and red color filters, see Figs. 5(a)-5(d). As these panels imply, overall, the resonance wavelength is shifted toward the blue region in both cases. These shifts are more pronounced in the MIMSI designs due to the larger optical path of light in these samples (compared to MIM ones). However, the color purity (peak shape and non-resonant response) is significantly modified in the MIM designs, while MIMSIs have kept their peak shape and FWHM width almost intact. This is due to the fact that in MIMSI structure the top insulator layer acts as a broadband antireflective coating that provides phase matching conditions in a broad wavelength and incident angles.

Overall, this work demonstrates the effectiveness of tandem shape FP designs in achieving optical behaviors that cannot be realized with common cavity designs. The high efficiency and color purity of these planar MIMSI designs, together with their large-scale compatibility bring them the opportunity to be scaled up for commercial applications.

Disclosures

The authors declare no conflict of interest.

References

1. C. Ji, K. T. Lee, T. Xu, J. Zhou, H. J. Park, and L. J. Guo, "Engineering Light at the Nanoscale: Structural Color Filters and Broadband Perfect Absorbers," Adv. Opt. Mater. **5**, 1–22 (2017).
2. D. Fleischman, L. A. Sweatlock, H. Murakami, and H. Atwater, "Hyper-selective plasmonic color filters," Opt. Express **25**, 27386–27395 (2017).
3. I. Koirala, V. R. Shrestha, C. S. Park, S. S. Lee, and D. Y. Choi, "Polarization-Controlled Broad Color Palette Based on an Ultrathin One-Dimensional Resonant Grating Structure," Sci. Rep. **7**, 40073 (2017).
4. Y. Gu, L. Zhang, J. K. W. Yang, S. P. Yeo, and C.-W. Qiu, "Color generation *via* subwavelength plasmonic nanostructures," Nanoscale **7**, 6409–6419 (2015).
5. Q. Xiang, Y. Chen, and Y. Wang, "Plasmonic reflection color filters with metallic random nanostructures," Nanotechnology **28**, 085203 (2017).
6. J. Wang, Q. Fan, S. Zhang, Z. Zhang, H. Zhang, Y. Liang, X. Cao, and T. Xu, "Ultra-thin plasmonic color filters incorporating free-standing resonant membrane waveguides with high transmission efficiency," Appl. Phys. Lett. **110**, 031110 (2017).
7. Y.-T. Yoon, H.-S. Lee, S.-S. Lee, S. H. Kim, J.-D. Park, and K.-D. Lee, "Color filter incorporating a subwavelength patterned grating in poly silicon.," Opt. Express **16**, 2374–2380 (2008).
8. M. J. Uddin, T. Khaleque, and R. Magnusson, "Guided-mode resonant polarization-controlled tunable color filters," Opt. Express **22**, 12307–12315 (2014).
9. M. J. Uddin and R. Magnusson, "Efficient guided-mode-resonant tunable color filters," IEEE Photonics Technol. Lett. **24**, 1552–1554 (2012).
10. Q. Wang, D. Zhang, B. Xu, Y. Huang, C. Tao, C. Wang, B. Li, Z. Ni, and S. Zhuang, "Colored image produced with guided-mode resonance filter array," Opt. Lett. **36**, 4698–4700 (2011).
11. C.-T. Wang, P.-C. Chang, J. J. Lin, M. C. Tai, Y.-J. Hung, and T.-H. Lin, "Full-color reflector using vertically stacked liquid crystal guided-mode resonators," Appl. Opt. **25**, 1248–1252 (2017).
12. E.-H. Cho, H.-S. Kim, B.-H. Cheong, P. Oleg, W. Xianyua, J.-S. Sohn, D.-J. Ma, H.-Y. Choi, N.-C. Park, and Y.-P. Park, "Two-dimensional photonic crystal color filter development," Opt. Express **17**, 8621–8629 (2009).
13. H. Cho, S. Han, J. Kwon, J. Jung, H.-J. Kim, H. Kim, H. Eom, S. Hong, and S. H. Ko, "Self-assembled stretchable photonic crystal for a tunable color filter," Opt. Lett. **43**, 3501 (2018).
14. W. Yue, S. Gao, S. S. Lee, E. S. Kim, and D. Y. Choi, "Subtractive Color Filters Based on a Silicon-Aluminum Hybrid-Nanodisk Metasurface Enabling Enhanced Color Purity," Sci. Rep. **6**, 29756 (2016).
15. K.-T. Lee, J.-Y. Jang, S. J. Park, C. Ji, L. J. Guo, and H. J. Park, "Subwavelength nanocavity for flexible structural transmissive color generation with a wide viewing angle," Optica **3**, 1489–1495 (2016).
16. A. Ghobadi, H. Hajian, B. Butun, and E. Ozbay, "Strong Light-Matter Interaction in Lithography-Free Planar Metamaterial Perfect Absorbers," ACS Photonics **5**, 4203–4221 (2018).
17. C. S. Park, V. R. Shrestha, S. S. Lee, and D. Y. Choi, "Trans-Reflective Color Filters Based on a Phase Compensated Etalon Enabling Adjustable Color Saturation," Sci. Rep. **6**, 25496 (2016).
18. Z. Li, S. Butun, and K. Aydin, "Lithography-free transmission fi lters at ultraviolet frequencies using ultra-thin aluminum films," J. Opt. **18**, 065006 (2016).
19. Z. Li, S. Butun, and K. Aydin, "Large-area, Lithography-free super absorbers and color filters at visible frequencies using ultrathin metallic films," ACS Photonics **2**, 183–188 (2015).
20. C. Williams, G. Rughoobur, A. J. Flewitt, and T. D. Wilkinson, "Single-step fabrication of thin-film linear variable bandpass filters based on metal–insulator–metal geometry," Appl. Opt. **55**, 9237–9241 (2016).
21. C. S. Park, V. R. Shrestha, S. S. Lee, E. S. Kim, and D. Y. Choi, "Omnidirectional color filters capitalizing on a nano-resonator of Ag-TiO2 -Ag integrated with a phase compensating dielectric overlay," Sci. Rep. **5**, 8467 (2015).
22. K. Mao, W. Shen, C. Yang, X. Fang, W. Yuan, Y. Zhang, and X. Liu, "Angle insensitive color filters in transmission covering the visible region," Sci. Rep. **6**, 19289 (2016).
23. C. Yang, W. Shen, Y. Zhang, K. Li, X. Fang, X. Zhang, and X. Liu, "Compact multilayer film structure for angle insensitive color filtering," Sci. Rep. **5**, 9285 (2015).
24. K. T. Lee, S. Y. Han, and H. J. Park, "Omnidirectional Flexible Transmissive Structural Colors with High-Color-Purity and High-Efficiency Exploiting Multicavity Resonances," Adv. Opt. Mater. **5**, 1700284 (2017).
25. K. T. Lee, S. Seo, J. Yong Lee, and L. Jay Guo, "Ultrathin metal-semiconductor-metal resonator for angle invariant visible band transmission filters," Appl. Phys. Lett. **104**, 231112 (2014).
26. V. R. Shrestha, S. S. Lee, E. S. Kim, and D. Y. Choi, "Non-iridescent transmissive structural color filter featuring highly efficient transmission and high excitation purity," Sci. Rep. **4**, 4921 (2014).
27. A. Ghobadi, H. Hajian, M. Gokbayrak, B. Butun, and E. Ozbay, "Bismuth-based metamaterials: From narrowband reflective color filter to extremely broadband near perfect absorber," Nanophotonics **8**, 823–832 (2019).
28. Z. Yang, Y. Zhou, Y. Chen, Y. Wang, P. Dai, Z. Zhang, and H. Duan, "Reflective Color Filters and Monolithic Color Printing Based on Asymmetric Fabry–Perot Cavities Using Nickel as a Broadband Absorber," Adv. Opt. Mater. **4**, 1196–1202 (2016).
29. A. Ghobadi, H. Hajian, M. C. Soydan, B. Butun, and E. Ozbay, "Lithography-Free Planar Band-Pass Reflective Color Filter Using A Series Connection of Cavities," Sci. Rep. **9**, (2019).
30. "Lumerical Solut. Inc. http://www.lumerical.com/tcad-products/fdtd/.," in *Lumerical Solut. Inc. Http://Www.Lumerical.Com/Tcad-Products/Fdtd/.* (n.d.).
31. Palik, "E. D. Handbook of optical constants of solids. Vol. 3 (Academic press, 1998)," (n.d.).